Received: 23 September 2021 | Revised: 22 November 2021 | Accepted: 29 November 2021

DOI: 10.1002/app.52013

ARTICLE

Applied Polymer SCIENCE WILEY

Engineering hybrid textile braids for tendon and ligament repair application

Tânia Peixoto[1,2] | Sofia Carneiro[1] | Raúl Fangueiro[3] | Rui M. Guedes[4] | Maria C. Paiva[2] | Maria A. Lopes[1]

[1]REQUIMTE-LAQV, Departamento de Engenharia Metalúrgica e Materiais, Faculdade de Engenharia, Universidade do Porto, Porto, Portugal

[2]Instituto de Polímeros e Compósitos, Departamento de Engenharia de Polímeros, Universidade do Minho, Guimarães, Portugal

[3]Centro de Ciência e Tecnologia Têxtil, Universidade do Minho, Guimarães, Portugal

[4]INEGI, Departamento de Engenharia Mecânica, Faculdade de Engenharia, Universidade do Porto, Porto, Portugal

Correspondence
Maria A. Lopes, REQUIMTE-LAQV, Departamento de Engenharia Metalúrgica e Materiais, Faculdade de Engenharia, Universidade do Porto, Rua Dr. Roberto Frias 4200-465, Porto, Portugal.
Email: malopes@fe.up.pt

Funding information
FCT/MCTES, Grant/Award Number: UIDB/50006/2020; Fundação para a Ciência e a Tecnologia, Grant/Award Numbers: PD/BD/143035/2018, UIDB/05256/2020, UIDP/05256/2020; European Social Fund; FCT - Fundação para a Ciência e a Tecnologia; Foundation for Science and Technology; Ministério da Ciência, Tecnologia e Ensino Superior

Abstract

Challenges involving tendon and ligament repair have motivated the investigation of new strategies to improve clinical outcomes. These have been mainly based on polymer constructs, which may be non-biodegradable or biodegradable. The former typically fails due to lack of device integration and the latter demands a complex balance between biodegradability and tissue ingrowth, often failing due to insufficient mechanical properties. This work presents the development of hybrid braids based on polyethylene terephthalate (PET) and polylactic acid (PLA) yarns. A textile technique was used to fabricate braids based on 16 multifilament yarns of varying PLA/PET composition. The composition was varied to maximize biodegradability while ensuring mechanical performance. The braids' morphology, physical and mechanical properties were characterized. As production parameters and architecture were maintained, the braids exhibited similar porosity and wicking ability. The breaking force and stiffness decreased significantly as the number of PLA yarns increased, although strain levels remained constant. Braids containing 10 and 12 PET yarns (out of the total 16 yarns) demonstrated good creep and force-relaxation behavior, as well as resistance to cyclic loading. These compositions were selected for future work, to be assembled into more elaborate structures to mimic the fibrous organization and tensile properties of different tendons/ligaments.

KEYWORDS

biodegradable, biomaterials, biomedical applications, fibers, textiles

1 | INTRODUCTION

Tendons and ligaments are fibrous connective tissues that perform crucial parts in transmitting forces from muscle to bone and bone to bone, respectively, providing, in this way, joint stability and allowing mobility.[1,2] Although these tissues present high tensile strength and stiffness,[2] due to the high mechanical demands placed upon them, the occurrence of injuries that compromise their mechanical integrity is very common, which ultimately results not only in pain, reduced activity, and disability to patients but in a serious economic burden as well.[1] Indeed, the annual global incidence of tendon and ligament ruptures and associated surgeries have been

Tânia Peixoto and Sofia Carneiro contributed equally to this work.

reported as 7–40 per 100,000 for Achilles' tendon (AT), 16–131 per 100,000 for rotator cuff tendons, and 8–50 per 100,000 for Anterior Cruciate ligament (ACL) repair. The costs of the initial repair, plus 3%–25% of these procedures necessitating revision surgery, ultimately represent tens of billions of dollars in the orthopedic clinical market.[2]

Due to low cellularity and insufficient blood supply, these tissues present an inadequate inherent healing capacity,[1,3] so clinical intervention is often needed to recover functional tissue integrity.[1] The repair can be performed by suturing the ruptured ends and augmenting the repair with biomaterials. In case of extensive tissue loss, it requires a biologic or synthetic graft with sufficient mechanical strength to replace the damaged tissue and bridge the gap.[1,3,4] Although reconstructions using auto- or allografts allow a better possible match for tissue properties, these present disadvantages, including the limited number of appropriate graft tissues, donor site morbidity, inflammatory response, or potential disease transmission.[1,5,6] Synthetic prostheses tend to present high strength, some even higher than that reported for human tissues, but long-term outcomes are not as good as expected.[2,4,5,7–10] These devices usually fail due to lack of either mechanical performance (e.g., rupture caused by wear, fatigue, and severe loading, device laxity, or loosening of the fixation element)[2,4,9] or by lack of biocompatibility in the long-term (e.g., inflammatory responses caused by wear particles, inferior device integration and lack of host tissue ingrowth into the structure).[2,4,7,9,11] Indeed, the adequate repair of these tissues is complicated mainly due to their unique non-linear and viscoelastic mechanical response and the complex organization of the collagen fibers in the structure, hierarchically grouped in several aggregation levels.[8,9] As a result, there is a clinical demand to investigate suitable solutions with improved biological/biomechanical properties to assure injured tendon/ligament tissue repair.[2,10]

The appropriate biomaterial and structural design of tissue scaffolds are crucial for the restoration of native functionality, thus determining the long-term success of the implant.[6,11,12] Ideally, a tendon/ligament scaffold should be compatible with the physiological environment and mimic the hierarchically aligned fibrillary microarchitecture of the native tissue to allow cells to attach and reproduce the extracellular matrix (ECM) components following the direction of alignment of the fibers. Also, it should act initially as a standard prosthesis to provide a mechanically stable initial structure but should be bio-resorbed in due time once the newly formed tissue is strong enough to withstand loading, allowing tissue growth and device integration with the adjacent host tissues. If the scaffold cannot survive the local loading environment, it can interfere with the natural regeneration mechanism, and there is a risk of early rupture. Ultimately, proper tissue formation does not occur.[1,6,13–15]

Synthetic materials, both absorbable and non-absorbable, have been studied for tendon/ligament repair scaffolds.[4] Non-degradable polymeric materials such as polypropylene (PP) and poly(ethylene terephthalate) (PET) present interesting mechanical properties for the envisaged application while also being biocompatible.[9,16] However, as previously mentioned, non-degradable devices present limitations, leading to the investigation of degradable substitutes.[4] According to the literature, the most commonly studied biodegradable synthetic materials for tendon/ligament engineering include polyesters such as polylactide (PLA), polyglycolide (PGA), and their copolymers.[1,17] However, some drawbacks that limit their use in biomedical applications are their mechanical performance, as these materials are mechanically weaker than healthy musculoskeletal tissues.[18,19] Also, biodegradable polymers as PLA fail prematurely at loading levels significantly lower than both the yield and the ultimate tensile strength of the material owing to viscoplastic flow originating creep rupture or fatigue failure.[20] Nevertheless, PLA may be a more beneficial scaffold material since it can maintain its mechanical properties for a longer period.[21]

Concerning the scaffold's morphology, it has been shown that textile-based scaffolds allow precise control of shape and size and result in good properties for the regeneration of these tissues.[6,22] Braided constructs are produced by the interlacement of three or more sets of yarns. These stand out due to their versatility in axial load-bearing properties, exhibiting good mechanical stability, high tensile strength, and fatigue resistance, making it an excellent structure for engineering connective tissues' scaffolds such as tendons and ligaments.[22–25]

Driven by this, our investigation group has developed non-degradable simple fibrous structures (braids) produced with PP or PET multifilament yarns using textile technology. The yarn type, yarns' number, take-up rate, and braiding angle were varied, consequently granting them different physical properties.[16] The necessity of proposing a device that presents biodegradability and the required mechanical properties has led the group to search for innovative solutions. As such, this work studies the possibility of using hybrid-braided structures composed of both PET and PLA multifilament yarns. The goal is to optimize the number of PLA yarns incorporated in the braids to allow their gradual degradation and integration within the host environment without compromising the mechanical performance. For this purpose, the hybrid structures produced were subjected to extensive

morphological, physical, and mechanical characterization. The hybrid braids with adequate properties will be further used as elementary parts and arranged into a more complex structure that mimics the microarchitecture of a specific tendon or ligament and its mechanical response. As the function of different tendons and ligaments varies according to their location, the requirements in terms of mechanical performance may not be as demanding for specific tissues. By tailoring the number of braids and the PET:PLA proportion in the final structure, it is possible to achieve many combinations, and the morphology (e.g., fibrous organization, thickness) and also actual load, strain at failure, and stiffness of different tendons/ligaments can be reached.

2 | MATERIALS AND METHODS

2.1 | Materials

PET multifilament yarn, with ~192 filaments and a linear density of ~1100 dtex, was purchased from Sarla Europe. PLA multifilament yarn, with ~108 filaments, and a linear density of ~1100 dtex, was purchase from Senbis Polymer Innovations.

2.2 | Production of braided textile structures

Braided structures were produced on a vertical braiding machine with 16 carriers, 16 yarns (Trenz Export Sa), and a take-up rate of ~3.96 cm/s, based on optimized conditions.[16] Different structures were produced by varying the proportion of yarn type (PET or PLA). The samples are named according to the number and yarn type present in 16PET, 12PET4PLA, 10PET6PLA, 8PET8PLA, 6PET10PLA, 4PET12PLA, and 16PLA. For example, 12PET4PLA is a braided structure with 12 PET yarns and 4 PLA yarns.

2.3 | Characterization of the polyethylene terephthalate and polylactic acid yarns

Scanning electron microscopy (SEM) was carried out in a FEI Quanta 400FEG microscope (ThermoFisher Scientific) to observe the PET and PLA multifilament yarns' morphology and determine the filaments' mean diameter.

Differential scanning calorimetry (DSC) analysis of each yarn was performed on DSC Netzsch equipment (Netzsch, Germany). PET yarns were heated from 30 to 300°C and PLA yarns from 30 to 200°C, at 10°C/min, under an N_2 atmosphere. The degree of crystallinity (χ_c) was determined from the thermal profiles obtained according to Equation (1):

$$\chi_c(\%) = \frac{\Delta H_m}{\Delta H_m^0} \times 100, \quad (1)$$

where ΔH_m represents the obtained melting enthalpy and ΔH_m^0 the melting enthalpy of 100% crystalline PLA ($93\,J\,g^{-1}$)[26] or 100% crystalline PET ($136\,J\,g^{-1}$).[27]

Tensile properties were measured using a Shimadzu EZ-LX Long-Stroke Model tensile testing machine (Shimadzu) with a 500 N load cell, with a gauge length of 235 mm and a crosshead speed of 8.5 mm/s, until failure. These conditions were used to simulate the length of a tendon (Achilles tendon, in particular) at a speed close to that of physiologic activities.[16,28,29] Although no specific standard was followed, the procedures adopted the recommendations of CY 1503-00 from Cordage Institute International Standard. The breaking force (N) was defined as the maximum force applied to the specimen carried to rupture, strain at break (%) as the strain of the test specimen produced by the breaking force, calculated by Equation (2):

$$\text{Strain at break}\,(\%) = \frac{\Delta L}{L_0} \times 100, \quad (2)$$

where ΔL represents the change in length of the specimen and L_0 its original length. Stiffness (N/mm) was calculated as the slope of the linear portion of the force (N)/elongation (mm) curve. Finally, breaking tenacity (cN/tex) was calculated by dividing the breaking force (cN) by the mean value of linear density (tex).

The yarn-on-yarn abrasion was performed following the CY 1503-00 from Cordage Institute International Standard, in a system where two portions of the yarn are intertwisted (three intertwisting wraps) and rub against each other under a controlled tension due to the cyclic motion (70 rpm) imposed by the rotation of a crank to which the yarn is attached. The tension is imposed by a weight representing ~2% of the yarn tensile maximum force and the number of cycles until the failure was recorded for samples tested in dry conditions and samples submerged in a phosphate-buffered saline (PBS) solution (pH = 7.4).

2.4 | Characterization of the polyethylene terephthalate, polylactic acid, and hybrid braided structures

Optical microscopy images of the different braided structures were obtained in a Leica microscope and analyzed

with ImageJ software to determine their diameter and braiding angle.

To estimate the porosity of the textile braids, three samples with 50 mm in length were considered. The geometrical volume (V_g) was determined considering the structures as a cylinder. Each yarn type in the structure was weighted separately to determine the theoretical volume (V_t), considering a cylinder composed of PET and/or PLA, where ρPET = 1.38 g/cm^3 and ρPLA = 1.24 g/cm^3. The porosity of the structure was then estimated according to Equation (3):

$$P(\%) = \frac{V_g - V_t}{V_g} \times 100. \quad (3)$$

The vertical wicking ability of the braids was also evaluated. Three specimens of each construct were tested, measuring 250 mm in length. The samples were suspended vertically with the extremity immersed in a reservoir with dyed distilled water. A clip was placed at the bottom end of each sample to guarantee that it could be immersed vertically at a depth of 30 mm. The wicking heights were measured every minute over 10 min.

Tensile mechanical properties of the braids were measured using a Lloyd instruments LR 30 K equipment with a 2.5 kN load cell, with a gauge length of 235 mm and a crosshead speed of 8.5 mm/s, until rupture. The stiffness (N/mm), breaking force (N), and strain at break (%) values of all structures were measured as described in the previous section. Tensile tests in wet conditions were also performed to determine if the braided constructs' mechanical strength was affected. Test specimens were immersed in 40 ml PBS until saturation (for 24 h) at 37°C. The remaining test conditions were the same as described above.

The evolution of the properties of the braided samples was also accessed through possible hydrolytic degradation. These assays were carried out using citric acid–Na_2HPO_4 buffer solution (pH 3) to accelerate the degradation process. Samples measuring ~800 mm in length were immersed in 40 ml solution and incubated at 37°C under 130 rpm. After one month, the samples were taken out from the container, washed with deionized water, and dried before subsequent characterizations. The samples were weighed, and the weight loss percentage was calculated by Equation (4):

$$\text{Weight loss}\,(\%) = \left(\frac{w_f - w_i}{w_i}\right) \times 100, \quad (4)$$

where w_i and w_f are the weight of the samples after the assay and weight of original samples, respectively. Tensile mechanical properties were accessed by tensile testing, as previously described.

The time-dependent behavior of the most promising braided structures was also evaluated. For creep testing, the braids were uniaxially loaded to 30%, 50%, and 70% of their breaking force in 20 s and kept at this level for 1000 s. After this holding phase, they were ramped down to reach 0 N after another 1000 s. As the permanent strain is an important aspect regarding the viscous response of polymers, after creep loading, this unloading stage was performed to measure the amount of recovered strain.[16] It is important to point out that the yield force was considered in the case of the 16PLA braid. The hybrid structures were also uniaxially loaded to 50% of the 16PET braid's breaking force and creep tested. For force-relaxation testing, the braided samples were elongated to 30%, 50%, and 70% of their strain at break in 20 s and then kept at this level for 1000 s. Both tests were performed on a Shimadzu EZ-LX Long-Stroke Model tensile testing machine (Shimadzu) with a 5 kN load cell and a gauge length of 235 mm. The braided structures were also exposed to cyclic loading up to 1000 cycles. The applied cyclic load, at a frequency of 0.1 Hz, was defined using a maximum load corresponding to 70% of their breaking force and a minimum load corresponding to 10%. The tests were performed in triplicate for each percentage on a Shimadzu EZ-LX Long-Stroke Model tensile testing machine (Shimadzu) with a 5 kN load cell and a gauge length of 235 mm. After applying these loading cycles, the samples were tensile tested according to the parameters previously described. However, before the tensile test, the braids rested ~24 h, since the strained rope will contract when it is allowed to rest unloaded, reaching equilibrium over a few hours, partially recovering the elongation.[9]

2.5 | Statistical analysis

Data are presented as mean value ± SD. Statistical analysis was performed using a one-way ANOVA test, and group differences were tested using t-tests in SigmaStat software. Differences were considered significant at a level of $p < 0.05$.

3 | RESULTS AND DISCUSSION

The design of scaffolds that can promote a functional repair of a tendon or ligament tissue requires the definition of the tissues' morphology and mechanical properties.[24] Fibrous scaffolds with hierarchically aligned structures and mechanical anisotropy resembling the biological tissue can provide a superior surface area for cell attachment, allowing their growth and production of

ECM components following the direction of fiber alignment, contributing to confer tendons' and ligaments' morphology and mechanical properties to the newly formed tissue.[23,24] Through textile technologies, it is possible to customize the desired properties by controlling the fibers' properties, such as size, geometry, orientation, pore size, and pore interconnectivity. In turn, these properties will contribute to determining cell behavior and the physical/mechanical properties of the final scaffold.[23,25]

This work reports the development and characterization of hybrid braids composed of PET and PLA, which can be later associated and arranged in different manners to form complex hybrid structures that mimic the fibrous architecture of different tendon/ligament tissues and their mechanical behavior. The goal is to take advantage of each complementary material, specifically, of the non-degradable material in providing good mechanical properties to ensure that the final structure has good mechanical performance to support the repair while the biodegradable material allows long-term tissue ingrowth and native integration, which is a common failure reported for the currently available non-degradable prosthesis. As a result, the presented strategy has potential to improve clinical outcomes where these standard repair strategies have failed and decrease the number of procedures necessitating revision surgery. The main focus was to study the number of PLA yarns incorporated in the braids that allow the adequate properties and does not compromise the braids' mechanical performance.

3.1 | Characterization of the polyethylene terephthalate and polylactic acid yarns

Yarn choice is usually the first step in building increasingly complex fibrous scaffolds and contributes to their final characteristics.[23,25] Compared to materials of natural origin, synthetic fibers present higher mechanical properties being interesting for the envisaged application. Their high robustness also allows their assembly using commercial textile machines.[25] Both PET and PLA were chosen in this work due to these reasons, along with the fact that both materials are biocompatible and have been studied as biomaterials in different medical applications.[1,16,17,21,30] Also, it has been reported that multifilament scaffolds may present increased mechanical properties, as these are usually stronger and present better elastic recovery than monofilament, which is likely due to load sharing between the several filaments that compose the structure.[31] When a particular load is reached, smaller defects appear on the several filaments composing the multifilament yarn, and even if some of the filaments fail, the others may keep the cohesion of the yarn and still withstand some load.[16] The lower flexural stiffness of multifilament scaffolds is also a positive aspect when used in a device to be implanted, as this would result in better conformability with the surrounding tissues, compared to a monofilament scaffold.[31] Also, multifilament scaffolds may provide superior surface area for cell attachment, higher wicking ability, and the possibility of smaller pores for infiltration of cells, which are essential properties for the tissue regeneration process, as will be later discussed.[16,31]

In Figure 1, SEM images of the PET and PLA multifilament yarns used in this study are presented. Both yarns are composed of several filaments aligned in parallel, presenting a smooth and homogeneous surface without defects. Based on the obtained images, the diameter of the filaments of each yarn was estimated, being 23 ± 1 μm in the case of PET and 34 ± 1 μm in the case of PLA. The estimated filament diameter of both yarns used in this work is attractive as it is reported that nanofibers and microfibers are capable of mimicking and promoting cellular alignment comparative with native tendon tissue. In contrast, inferior cellular reorganization is observed for thicker fibers (>100 μm).[32]

The fibers' crystallinity degree affects their physical–mechanical characteristics and biodegradability.[33] To evaluate the crystallinity of PET and PLA multifilament yarns, their thermal properties were evaluated by DSC analysis. Figure 2 presents the obtained thermograms.

The onset of melting obtained for the PET yarn was around 239°C, while for PLA was around 152°C. PLA and PET present a double melting peak, indicating the presence of two crystalline forms that developed during fiber melt processing and yarn production. The multiple melting behavior of PET and PLA homopolymers was studied by several authors.[34–37] Three endotherms were identified: a first at lower temperature (frequently not detected), a second associated with the melting of secondary crystals and partial melting of less stable primary crystals, and a third mostly associated with the melting of the stable primary crystals. The structural complexity increases for fibers, which present a highly anisotropic structure inducing macromolecular orientation along the fiber axis, and possibly affecting crystallinity. These complex effects continue under investigation, and few studies are reported in the literature.[38]

From the area of the melting peak, the melting enthalpy (H_m) was calculated, and based on the previously described Equation (1), the crystallinity (χ_c) of both yarns was estimated, which for PET was ~37% and for PLA was ~50%, indicating that both polymers present crystalline domains.

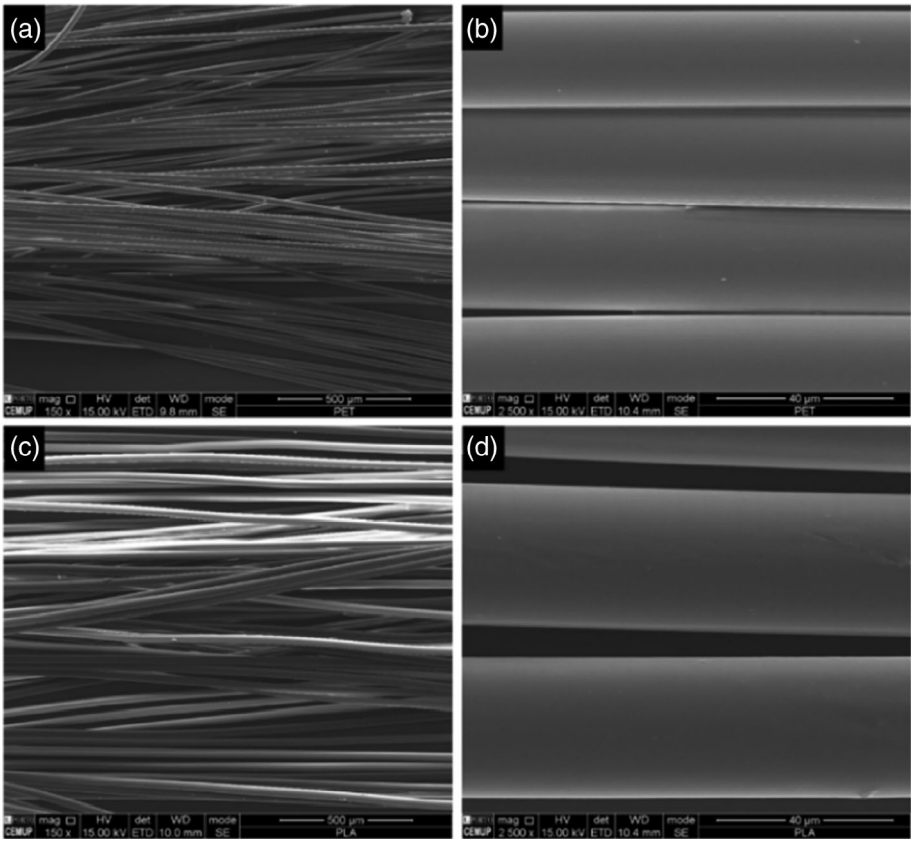

FIGURE 1 Scanning electron microscopy images of polyethylene terephthalate multifilament yarn: (a) 150× and (b) 2500×, and of polylactic acid multifilament yarn: (c) 150× and (d) 2500×

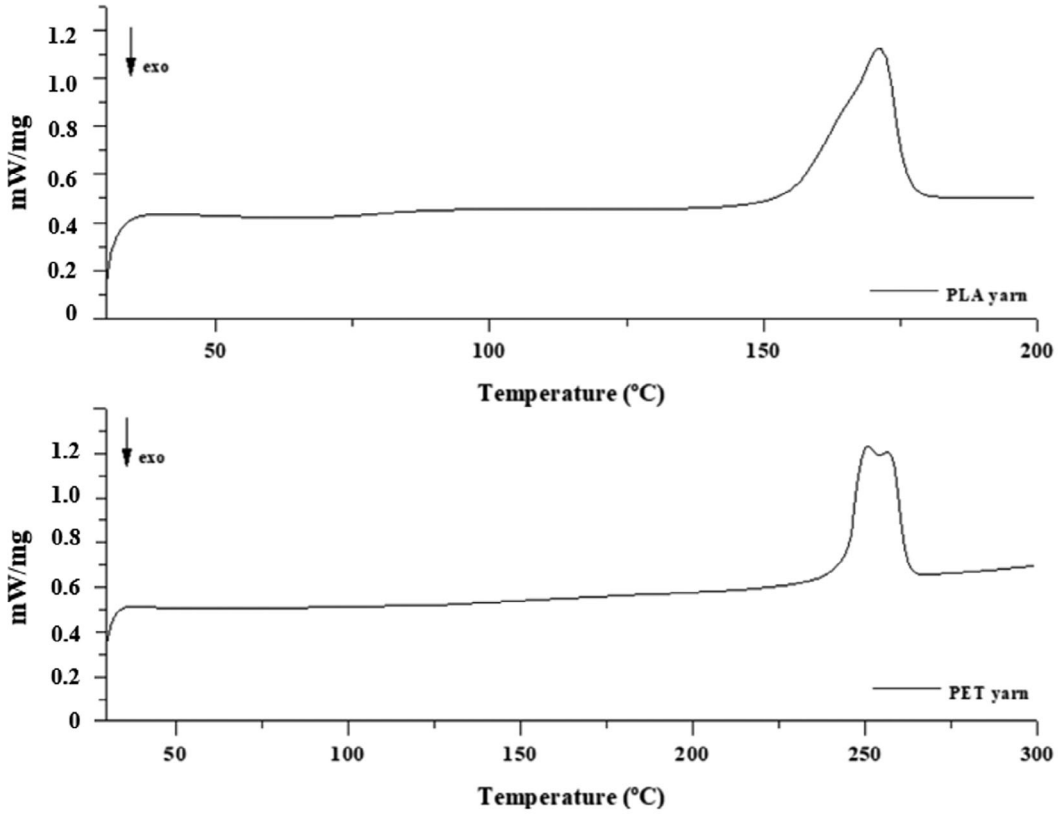

FIGURE 2 Differential scanning calorimetry results illustrating thermograms for polyethylene terephthalate and polylactic acid yarns

Figure 3a shows representative force/strain curves of both PET and PLA multifilament yarns, depicting distinct shapes, indicating a difference in mechanical behavior. The force–strain curve of the PLA yarn shows an initial region of Hookean behavior, followed by a well-defined yield zone. Above ~2.7% strain, a small region of elongation without an increase in force is immediately followed by strain-hardening behavior observed as a steady increase in force with elongation, ending with yarn failure at deformation near 30.5%. Rupture was observed to occur in steps suggesting a progressive break of the filaments that compose the yarn. The PET yarn shows the initial linear force–strain relation with a higher slope than PLA up to approximately 1.5% strain, indicating a higher Young's modulus. It is followed by a decrease in slope up to 5% strain, increasing fast until breaking strain, with a breaking force that more than doubles that of PLA, demonstrating to be a stronger fiber. Figure 3b compares the breaking force, strain at break, stiffness, and breaking tenacity values obtained for both fibers, illustrating the higher tensile properties of the PET yarn, significantly different from the PLA yarn. The different melt-spinning conditions during the production of both yarns may have influenced the presented mechanical properties. Due to the higher levels of molecular orientation attained at higher draw-ratios, stiffness increases but the opposite effect occurs with strain at break. Nevertheless, these results are in line with the literature, as it is reported that the mechanical properties of PLA are generally inferior to other polyesters.[39] The difference in yarn properties hereby observed will reflect on the tensile behavior of the hybrid braids, as will be discussed below.

Abrasive wear in textiles can occur during usage due to friction between their fibrous components and can be critical in a fibrous structure to be implanted in the human body, as it may result in device rupture or in unwanted inflammatory responses originating from the wear particles, impairing the healing process, as mentioned before. Inter-yarn abrasion is considered one of the principal causes of short life or failure of synthetic ropes during tension and bend cycling. Abrasion is related to the physical destruction of yarns and textiles due to the repetitive rubbing of a surface over another, resulting in heating and the loss of performance (e.g., mechanical damage).[40,41] Frictional forces developed in the yarn due to the motion of the test are dissipated in the filaments by developing tensile and shear stresses, and repetition of such stresses eventually causes filament fatigue, which results in the loss of mechanical properties, and eventually rupture.[42] This property was also accessed as abrasion resistance of the used yarns and contributes to predict the performance of the final fibrous structure.

When tested under dry conditions, PLA yarns could withstand 9950 ± 1548 cycles until rupture, while PET yarns could withstand 29,038 ± 5935 cycles. When submerged in PBS solution, the abrasion resistance of PLA yarns decreased by 88%, resisting 1164 ± 416 cycles until rupture. The wet abrasion resistance of the PET yarns decreased by 34%, being able to withstand 19,206 ± 5376 cycles. The obtained results illustrate that the PET yarns show overall enhanced abrasion resistance under both test conditions compared to PLA yarns.

The abrasion resistance of the yarn is affected by different factors, such as the intrinsic abrasion resistance of the fiber composing the yarn (raw material) and its geometry.[43,44] Indeed, abrasion in yarns is related to properties such as polymer chemistry and molecular weight, crystalline structure, and characteristics such as linear density, yarn size, and cohesiveness.[40,43,44] Usually,

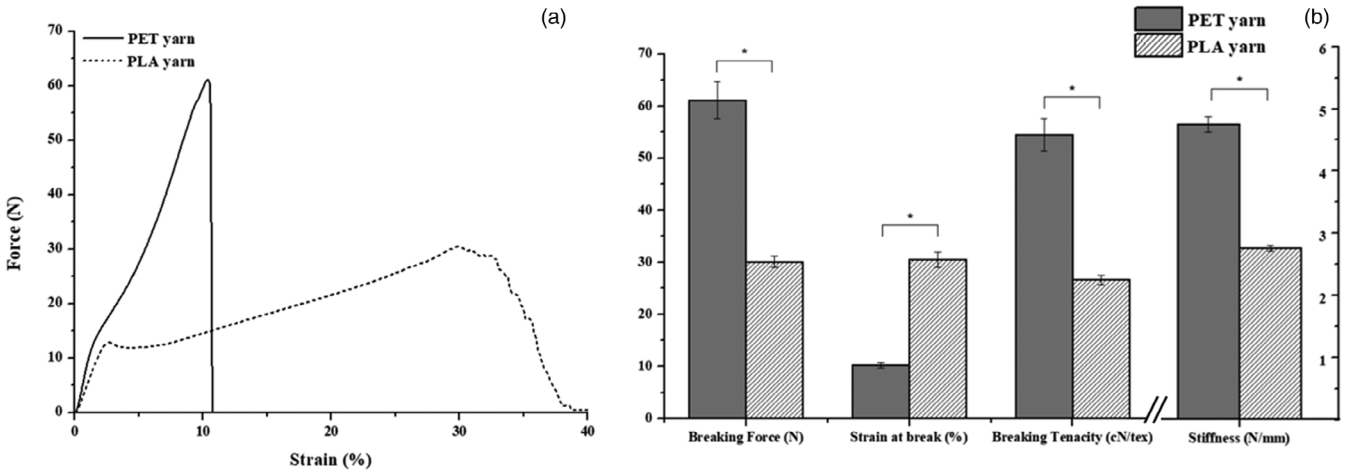

FIGURE 3 (a) Force/strain curves of the polyethylene terephthalate (PET) and polylactic acid (PLA) multifilament yarns; (b) graphic representation of the measured tensile properties (* $p < 0.05$); the scale on the right refers only to the stiffness

PLA presents poor abrasion resistance compared, for example, to PET.[45,46] The mechanical properties of the constituent material are important for abrasion. It is generally accepted that using a stronger and stiffer material leads to a stronger yarn, and it is expected that similar assumptions are valid for yarn abrasion,[47] as abrasion is recognized as a repeated application of stress and, therefore, a capacity to absorb the stress is required on the entire yarn structure.[42] Indeed, in this study, PET yarns demonstrated superior tensile properties (namely breaking force and stiffness), as previously reported, which may contribute to its increased abrasion resistance. In addition, as the PET yarns present thinner filaments, there is higher cohesion between them during abrasion, and, as a result, there is a smaller total surface to be abraded, which also contributes to the better abrasion resistance of the yarn.[40]

PLA is known for its biodegradability, and the main factor of PLA degradation is hydrolysis.[48] Polyesters hydrolyze by breakage of the ester bonds in the presence of water, leading to chain scission and formation of a low molecular weight alcohol and carboxylic acid end groups in the polymer. While PET typically requires alkaline conditions for hydrolysis to occur, PLA is prone to hydrolysis in the presence of a small concentration of water alone. The rate of hydrolysis is affected by the imposed stress and temperature conditions, leading to molecular weight reduction and weakening of mechanical properties.[20,48,49] Although to a less extent, PET may also undergo hydrolytic degradation under the combined action of water and temperature.[50,51] This chain scission leads to a decrease in the molar mass of the polyester, and consequently, a loss of mechanical properties.[50,52] During the abrasion process, the friction induces an energy transfer to the surface molecules, resulting in a local temperature increase. Along with the imposed stress, these factors may promote the degradation of the yarns, decreasing their abrasion life under wet conditions. Consequently, it is expected that the number of PLA yarns in the implantable fibrous structure is critical for its mechanical performance and durability. Thus, the best PET/PLA composition should be assessed to provide a good balance of properties for the target application.

3.2 | Characterization of the polyethylene terephthalate, polylactic acid, and hybrid braided structures

The optical microscopy images of PET, PLA, and the different hybrid braided constructs, with the estimated diameter and braiding angle values, are presented in Figure 4. Based on the yarns' orientation, the produced structures are classified as biaxial, presenting two sets of yarns placed in the clockwise and anti-clockwise direction.[53,54] The type of interlacement is classified as regular since the yarns were crossed alternatively over and under yarns in opposite directions, with the rotation being two by two (2/2 repeat).[53–56] During the production of the hybrid structures, the PET yarn carriers were successively replaced in pairs by the PLA ones, one in each braiding direction.

All structures present very similar values regarding their braiding angle, and only a slight difference was noted in the diameter of the structures with more PLA, particularly beyond the 8PET8PLA braid. The braid angle, defined as the angle formed by the intertwining yarn with the braid axis, varies with parameters such as yarn thickness, braiding machine speed (related to the movement of the yarn carriers), and take-up speed,[53,55] and strongly influences the mechanical behavior of braided structures.[57] The braid diameter is modulated by variables such as the number of yarns, braiding angle, number of fiber intersections per unit length of the yarns, and linear density (tex).[56] Since all the braids were produced under similar processing conditions, specifically the same take-up rate, the major factor that could lead to variations in the braiding angle and braid diameter was the yarn type.

The porosity of the braided structures, which is essentially the measure of the void space,[23] did not present a relevant variation among the braids, ranging from 80% to 83%. The structures with higher PLA content (≥8PLA yarns) presented slightly higher porosity than the 16 PET braid, probably due to their slightly higher diameter. The porosity of a textile scaffold may be controlled at different levels: the inter-filament gap (adjusted by changing the number of filaments in the yarn, their diameter, and the yarn-packing density), and the gap between yarns.[23] As previously explained, the linear density of the PET and PLA yarns is similar, and the braids' production conditions were the same, so it was not expected that there would be large differences between the samples.

Wicking refers to the ability of a liquid to wet fibers assembled into textile structures based on the capillarity phenomenon. It involves the spontaneous wetting of the fibrous network, occurring when the fibers are assembled with capillary spaces between them and through pores. Wicking depends on the properties of the liquid, the liquid-surface interactions, and the geometry of the capillary and pore structures.[58,59] The braided structures' wicking profile is presented in Figure 5.

The rate of water rise was higher in the initial period, and after that, it slowed down gradually, which may be due to the effect of gravity on the mass of rising water. As the PLA content in the structure increased, the liquid

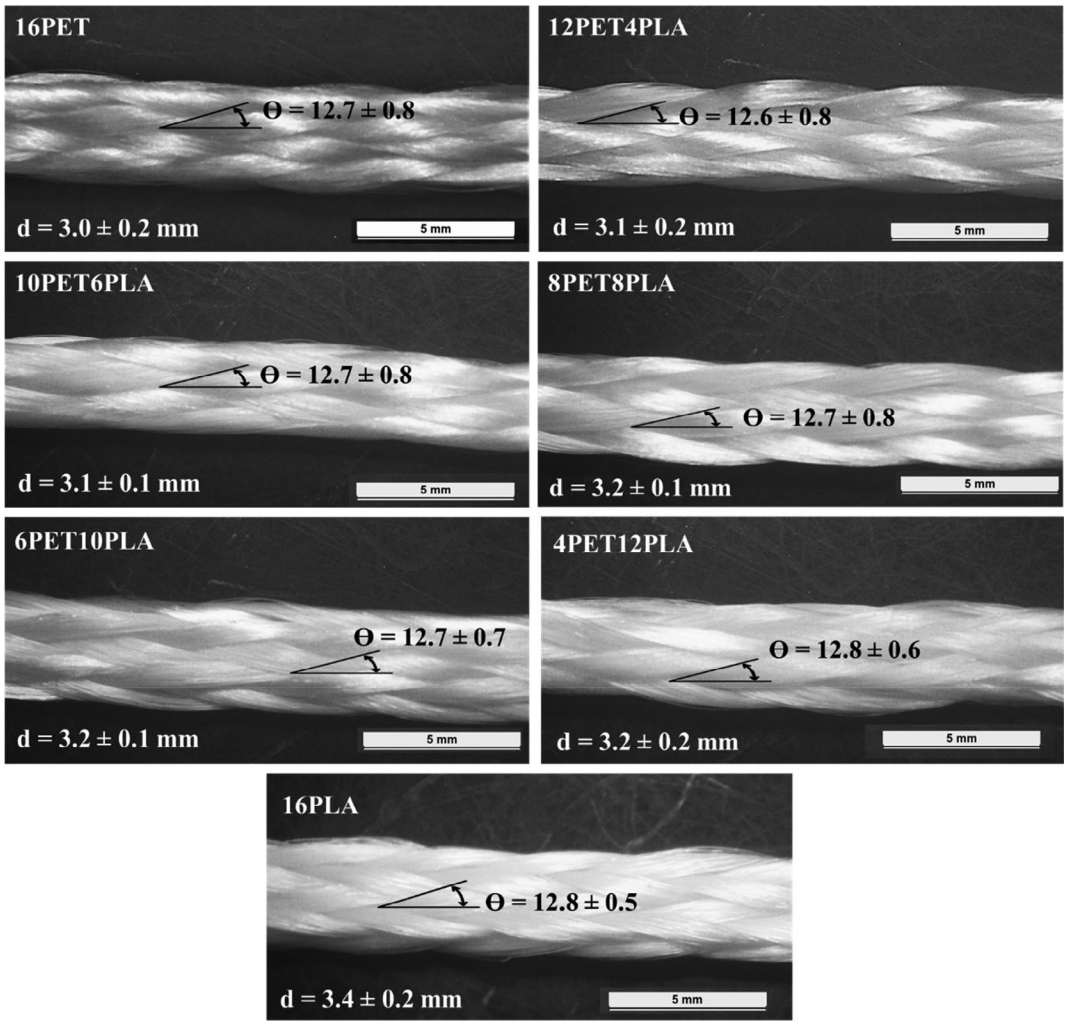

FIGURE 4 Optical microscopy images of polyethylene terephthalate (PET), polylactic acid (PLA) and hybrid braided structures; the composition is identified on the top left of the images; the scale bar indicates a length of 5 mm

transport capacity also seemed to increase initially. After 10 min, the test ended since all structures reached a similar height value of ∼19 cm, almost the entire braid testing length, except for 16PET, which reached a value of ∼17 cm. As mentioned above, wicking depends on factors such as fiber composition, structure, pore size, and distribution[59] so that a small pore size and evenly distributed, interconnected pores, originate faster wicking.[59] The PET and PLA yarns are formed by filaments of different sizes, each containing a different number of filaments, which may contribute to the formation of pores with different sizes and distribution, leading to different capillary pressure effects in the presence of water.

Braided textile structures tend to present uniform pore distribution, with excellent reproducibility of porosity, which usually ranges from 30% to 90%, while also presenting excellent pore connectivity.[23] For tissue repair, a scaffold needs to have a high porosity level and good pore interconnectivity. These conditions provide an ideal physical environment for cell infiltration, a larger surface area for cellular attachment, growth, and proliferation. In addition, the circulation of biological fluids, nutrients as oxygen and growth factors, and other metabolites is facilitated upon implantation, as neovascularization. These conditions are essential to assist in guiding and promoting tissue ingrowth.[11,15,23,24,32]

As previously explained, recovering the mechanical performance of a ruptured tendon/ligament tissue using a medical implant is challenging but important.[60] Adequate implant properties are required to maintain integrity after implantation and support the necessary dynamic loads in vivo until sufficient host tissue growth has occurred.[21] To achieve that, a strong and stiff material demonstrating non-linear tensile mechanical behavior similar to the native tissues is necessary.[60] Thus, the tensile properties of the braids produced, intended for use as parts of a more complex structure-supportive scaffold to repair a tendon/ligament, were investigated.

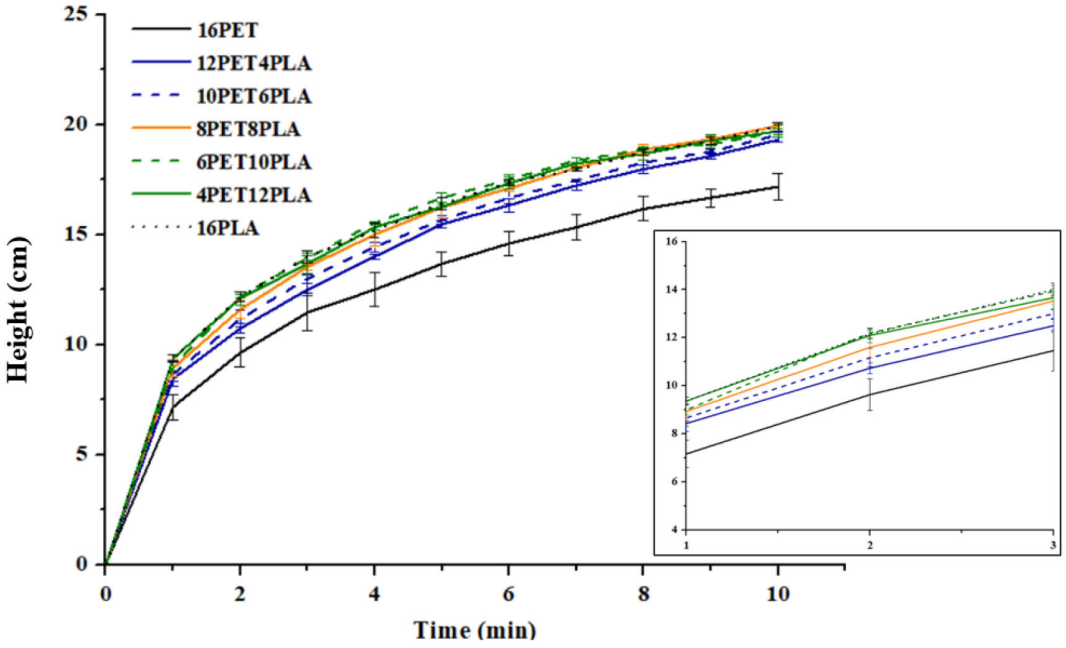

FIGURE 5 Water height along the braided structures over 10 min. The inset image illustrates a higher magnification from test minute 1 to 3 [Color figure can be viewed at wileyonlinelibrary.com]

Figure 6a illustrates the force/strain curves obtained for the braided constructs in the dry state, and Table 1 summarizes the tensile results obtained. Similar to the native tissues, these braided constructs also display a non-linear force–strain behavior. A curved portion is observed, in which the braid undergoes geometric transition as a response to the application of load, being subsequently followed by a linear region in which the yarns' properties govern the tensile response until rupture.[54] It can be observed that the 16PET braid presented a portion of the curve (until the breaking force) similar to that of hybrid structures that is, with similar deformation but different values of breaking force. Indeed, as observed in Figure 6b, the breaking force is reduced significantly among samples by increasing the PLA content in the braid. As shown in Figure 6c, the 16PET and hybrid structures all exhibited similar strain at break values, because the initial rupture of the hybrid braids occurs with the rupture of the PET yarns. After this point, the PLA yarns in the hybrid braids still sustained load, breaking progressively with significant plastic deformation before a complete rupture of the braid occurred. Indeed, the tensile behavior of the 16PLA braid shows a defined yield zone followed by considerable plastic deformation before failure. Stiffness values (Figure 6d) also showed a decreasing trend with the increase in PLA in the structure. The obtained results are in accordance with the tensile properties of the single material yarns, and their combination reflects the contribution of each material.

The tensile properties of a hybrid structure will depend on the properties of the components. Due to their higher stiffness, most of the applied load is shielded by the PET yarns. After their rupture, there was only residual maintenance of the load by PLA until the failure of the rest of the structure (Figure 7). As such, the decrease in breaking force and stiffness values with the increase in PLA content mainly results from the fact that there are fewer PET yarns available in the hybrid braid to withstand the applied load. In conclusion, the presented tensile results indicate that the PET yarns are the primary providers of tensile strength for the produced hybrid braids.

To investigate the effect of hydration on the tensile properties, braids saturated in PBS under physiological temperature conditions were also tested. The obtained results are depicted in Table 2, and Figure 8 compares the results obtained for the tensile properties of the braids under dry and wet conditions. The breaking force and strain values of the braids with higher PLA content (6PET10PLA, 4PET12PLA, and 16PLA) were significantly different under dry and hydrated conditions. In contrast, no major difference was observed for the tensile properties of the 16PET braid and hybrid braids 8PET8PLA, 10PET6PLA, and 12PET4PLA. These results may be due to the level of PET's hydrophobicity compared to PLA, which may have resulted in higher liquid affinity and absorption, leading to lower strength and strain. Nevertheless, stiffness values did not change in wet conditions.

Based on the previous findings obtained by the group,[9,16] the minimum values for strength and stiffness to fulfill the intended application requirements should

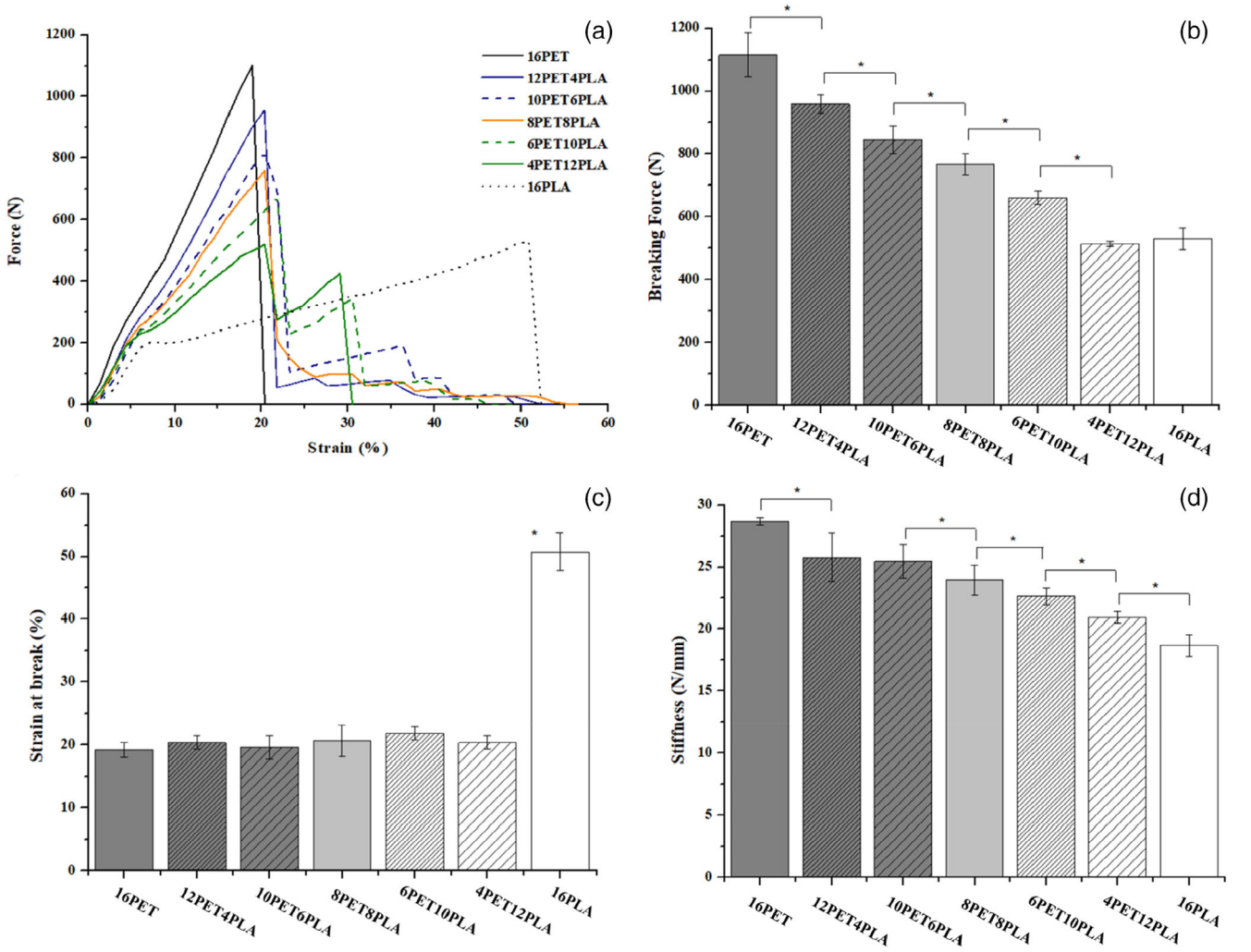

FIGURE 6 (a) Force/strain representative curves of the braided structures; results obtained for (b) breaking force (N), (c) strain at break (%) and (d) stiffness (N/mm) of the braided structures (* $p < 0.05$) [Color figure can be viewed at wileyonlinelibrary.com]

TABLE 1 Tensile properties of the produced braided structures (dry conditions)

Sample	Breaking force (N)	Strain at break (%)	Stiffness (N/mm)
16PET	1116.3 ± 68.9	19.2 ± 1.2	28.7 ± 0.3
12PET4PLA	958.8 ± 28.7	20.4 ± 1.1	25.8 ± 1.9
10PET6PLA	845.4 ± 45.3	19.7 ± 1.8	25.5 ± 1.4
8PET8PLA	766.8 ± 35.1	20.7 ± 2.5	24.0 ± 1.2
6PET10PLA	662.0 ± 21.2	21.9 ± 1.0	22.7 ± 0.7
4PET12PLA	513.3 ± 8.2	20.4 ± 1.0	21.0 ± 0.5
16PLA	529.7 ± 34.7	50.8 ± 3.0	18.7 ± 0.9

approximate the ones of the 16PET braid. As the decrease in strength and stiffness is greater than 40% and 20%, respectively, in the hybrid braids with more PLA content than PET, only the other hybrid braids (8PET8PLA, 10PET6PLA, and 12PET4PLA) were selected for further characterization. 16PET and 16PLA braids were also characterized to serve as controls.

The possible effects of hydrolytic degradation on the weight and tensile properties of the produced braids were evaluated, following a protocol for accelerated degradation testing. For the sake of time-saving, an accelerated degradation test was performed, for one month, in a pH 3 solution, as the pH can have a substantial influence on PLA degradation since it acts both

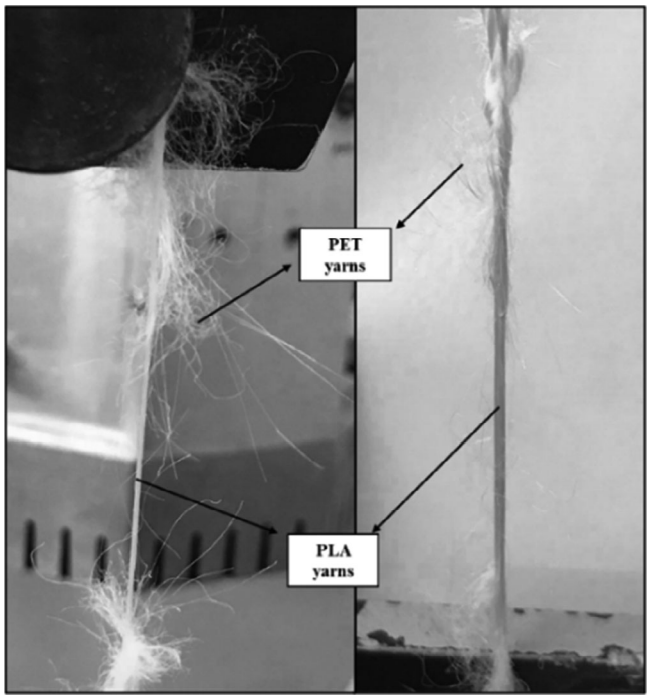

FIGURE 7 8PET8PLA braid structure after the maximum breaking force was attained. This illustrates the remaining polylactic acid (PLA) yarns during tensile test, after polyethylene terephthalate (PET) failure has occurred

on the reaction mechanism and on the reaction kinetics.[49]

No significant weight loss was observed for all the braids throughout the study. Figure 9 shows the results of the tensile tests conducted on the braids after one month in a pH 3 solution compared to the tensile results previously obtained in dry conditions. It can be observed that the 16PET and hybrid braids tested for possible hydrolysis showed marginal alterations of the tensile properties, while a slight increase in stiffness was observed for the 16PLA braid.

While PET is labeled as non-biodegradable[61] and has gained wide acceptance over the yarns for exhibiting excellent biostability after implantation,[62] PLA is considered biodegradable, presenting a slow degradation rate, taking from months to a few years for total in vivo resorption, depending on parameters such as crystallinity, molecular weight or material morphology.[20,63,64] The previously reported yarns' crystallinity contributed to the structure's stability under the tested hydrolysis conditions since degradation begins in the amorphous regions, while the ordered structure of the crystalline regions shield the polymer from the degradation factors.[20,49,64,65]

As the braids under study are intended to form part of a structure for tendon/ligament repair, this is a

TABLE 2 Tensile properties of the produced braided structures (wet conditions)

Sample	Breaking force (N)	Strain at break (%)	Stiffness (N/mm)
16PET	1109.6 ± 93.1	19.0 ± 2.7	28.6 ± 1.0
12PET4PLA	959.2 ± 32.7	19.3 ± 0.7	25.8 ± 0.9
10PET6PLA	850.6 ± 26.9	19.0 ± 0.0	25.4 ± 0.3
8PET8PLA	732.8 ± 17.4	18.6 ± 0.7	24.6 ± 0.9
6PET10PLA	599.9 ± 45.0	17.0 ± 1.7	23.1 ± 0.7
4PET12PLA	501.5 ± 44.3	17.5 ± 1.5	21.7 ± 0.7
16PLA	476.5 ± 30.4	39.9 ± 2.5	19.1 ± 1.4

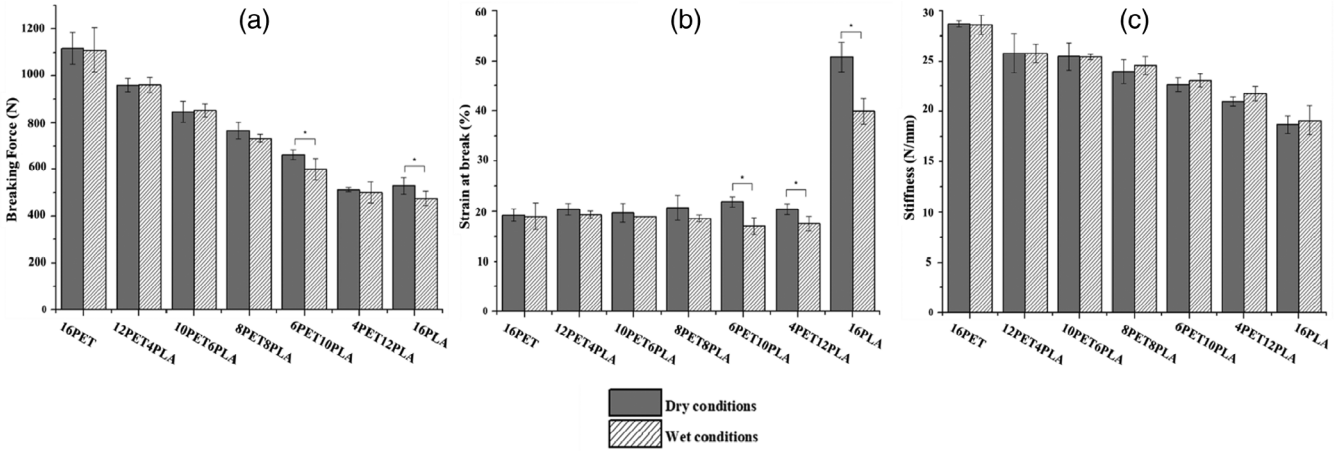

FIGURE 8 Tensile testing results of wet braids: (a) breaking force (N), (b) strain at break (%) and (c) stiffness (N/mm) (* $p < 0.05$)

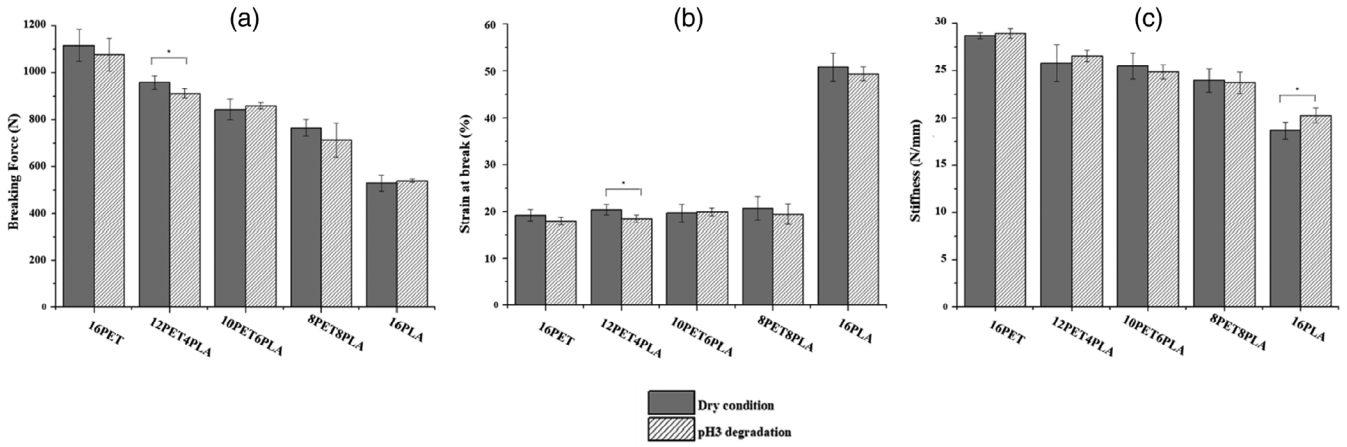

FIGURE 9 Tensile results of braids after accelerated degradation: (a) breaking force (N), (b) strain at break (%), and (c) stiffness (N/mm) (* $p < 0.05$)

relevant aspect. Although the duration of the repair process depends on the location and severity of the injury, it is stated that this process is slow compared to other musculoskeletal tissues, with sufficient tissue repair taking more than a year.[2,64] Thus, the biodegradable portion of the synthetic prosthesis must preserve its properties along this term until the functionality of the newly formed tissue has been achieved, being slowly degraded while fulfilling its purpose.[23,64] Even though it was previously concluded that the PET yarns might be the primary providers of mechanical strength in the braids, the observed capacity of the PLA yarns to maintain their integrity and structural properties is essential for them to be able to support and guide the repair until necessary. Nevertheless, more realistic in vitro studies on the final structure composed by these braids and, of course, in vivo assays will have to be performed to confirm the obtained results since it cannot be guaranteed that these will remain valid after implantation.

To complete the mechanical characterization of these materials, it is necessary to consider the stability of the braids' properties over time under repeated dynamic loading to simulate the conditions that the native tissues experience under physiologic conditions. When a tendon or ligament is under load, it will display a viscoelastic behavior, exhibiting force-relaxation, creep, and mechanical hysteresis.[66,67] These properties were evaluated for selected braided structures. Creep and relaxation tests were performed at three different load and strain levels.

Creep measurements are of great interest in any application where the polymeric material must sustain loads for extended periods.[68] The creep phenomenon means that the deformation caused by a constant load increases over time until a steady-state value is reached.[66,67,69] When a viscoelastic polymer is subjected to a constant load, an instantaneous elastic deformation is initially observed, followed by a time-dependent strain, which is curved at the beginning and eventually reaches a limiting slope. After the load is removed, a recovery process occurs until a permanent deformation is observed due to the viscoplasticity, that is, time-dependent irreversible deformation.[68]

As observed in Figure 10a, the greater the applied force for each braid sample, the higher the deformation that the structure undergoes, as expected. When observing the creep behavior in a log–log scale (Figure 10b), it becomes clear that for the 16PET, 12PET4PLA, 10PET6PLA, and 8PET8PLA braids, the evolution of strain was linear. A low creep rate was observed for all levels, although a slight increase in slope during the 1000s holding period was noticed as the PLA content in the structure increased. Considering the 70% loading level, for example, and concerning the initial strain value ($t = 20$s), the strain level of the 16PET braid increased from ~15.5% to ~16.9%, giving a creep of ~1.4%. This value was similar for the 12PET4PLA (~ 1.5%), increasing for the 10PET6PLA braids (~1.9%), while the 8PET8PLA braid creeped ~2.1%. This slight difference was expected since by increasing the stiffness of the chains, a better creep resistance of the material is achieved.[69] As previously observed in tensile testing, stiffness tends to decrease with increasing PLA content. Indeed, it can be observed that the 16PLA braid demonstrated high creep (~6.3%), even when subjected to only 70% of its yield force. Polymers such as PLLA are reported to creep at applied strains that are lower than the yield strain, which can have a crucial consequence on the behavior of the scaffold structure.[20] Hawkins et al.[70] reported an increase from 0.3% in the strain at the start of the activity to 3.3% after seven minutes of Achilles tendon stimulation, giving a total dynamic creep of 3.0%. Except

for the 16PLA braid, the creep rates displayed by the other braids are below this reported value, which constitutes a positive creep behavior, considering the final application of the structure, which will be exposed to different loadings over long periods, and should not become lax.

The values of the permanent strain (ε_p) and the recoverable strain (ε_r) are presented in Table 3. The observed permanent strain due to some plastic deformation of the yarns is low and similar between the 16PET and hybrid structures for each creep level. PLA only recovered about 30% for the tested level.

When the hybrid structures are loaded to 50% of the breaking force of the PET braid (Figure 11a), the structures with higher PLA content achieved higher strain levels after initial loading. All hybrid structures present a low creep rate, although, as before, a slight increase in slope during the 1000s holding period was noticed as the PLA content in the structure increased. For this loading level, the 16PET creeped about 1.2%, the 12PET4PLA displayed a creep rate of ~1.4%, while the 10PET6PLA and 8PET8PLA creeped ~1.6% and 2.3%, respectively. After the unloading period, the recovery level was similar for all structures.

Nevertheless, it is important to point out that by analyzing the morphology of the hybrid braids after the test, especially the ones with higher PLA content (8PET8PLA braids), it was possible to observe the higher deformation and loosening of the PLA yarns in the structures, which may become plastically deformed (Figure 11b). These changes were also

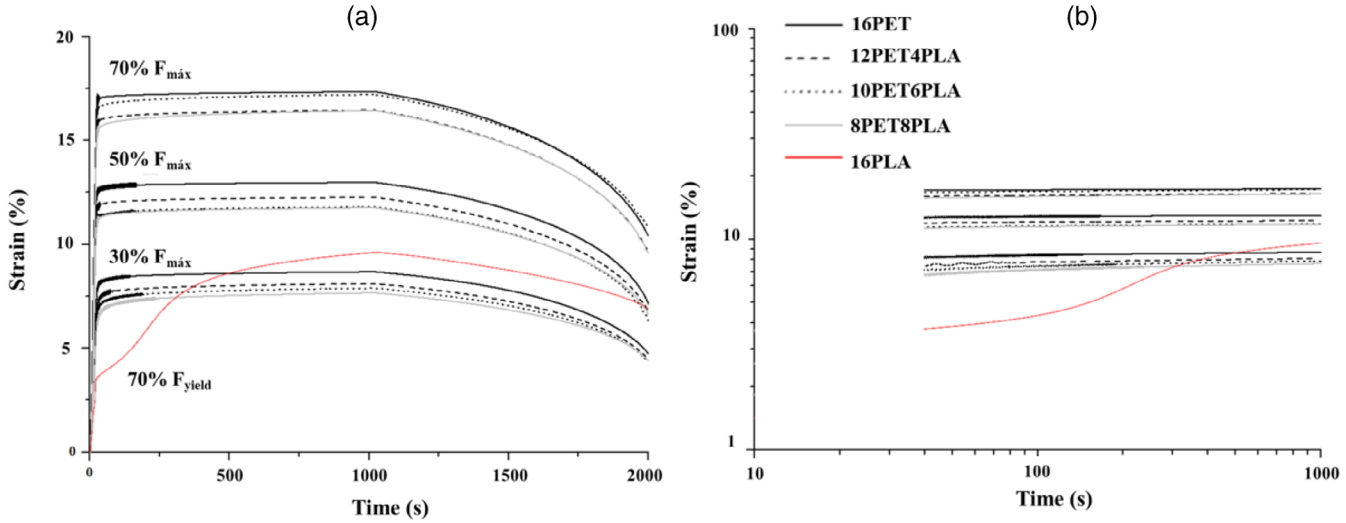

FIGURE 10 (a) Representative curves of creep/recovery behavior of the braided structures at different levels of force; (b) in Log–Log scale [Color figure can be viewed at wileyonlinelibrary.com]

		Creep level (%)		
Structure	**Strain (%)**	**30**	**50**	**70**
16PET	$\varepsilon_p = \varepsilon_t \approx 2000$ s	4.2 ± 0.8	5.3 ± 0.3	7.4 ± 0.7
	$\varepsilon_{max} = \varepsilon_t \approx 1000$ s	8.8 ± 0.6	12.4 ± 0.5	16.9 ± 0.5
	$\varepsilon_r = \varepsilon_{max} - \varepsilon_p$	4.5 ± 0.3	7.1 ± 0.3	9.5 ± 0.3
12PET4PLA	$\varepsilon_p = \varepsilon_t \approx 2000$ s	3.6 ± 0.1	5.7 ± 0.3	7.4 ± 0.5
	$\varepsilon_{max} = \varepsilon_t \approx 1000$ s	7.9 ± 0.2	12.5 ± 0.4	16.9 ± 1.1
	$\varepsilon_r = \varepsilon_{max} - \varepsilon_p$	4.3 ± 0.2	6.8 ± 0.2	9.6 ± 0.6
10PET6PLA	$\varepsilon_p = \varepsilon_t \approx 2000$ s	4.3 ± 0.8	5.5 ± 0.4	8.1 ± 0.3
	$\varepsilon_{max} = \varepsilon_t \approx 1000$ s	8.7 ± 1.1	12.5 ± 0.8	17.6 ± 0.4
	$\varepsilon_r = \varepsilon_{max} - \varepsilon_p$	4.4 ± 0.3	7.0 ± 0.6	9.5 ± 0.1
8PET8PLA	$\varepsilon_p = \varepsilon_t \approx 2000$ s	3.8 ± 0.2	6.2 ± 0.7	8.0 ± 0.4
	$\varepsilon_{max} = \varepsilon_t \approx 1000$ s	7.7 ± 0.2	12.7 ± 0.9	17.1 ± 0.9
	$\varepsilon_r = \varepsilon_{max} - \varepsilon_p$	3.9 ± 0.0	6.6 ± 0.3	9.1 ± 0.6

TABLE 3 Permanent strain (ε_p) and recoverable strain (ε_r) of the braids for each creep level

observed in the previous testing conditions, and as the creep level increased (from 30% to 70%), it would become more noticeable. It appeared that as more PET yarns are present in the structure, the less visible this effect would be. These results complement the previous observations that the PET yarns are the primary providers of mechanical properties for the produced hybrid braids.

Force-relaxation means that the force necessary to maintain a constant elongation decreases over time, and this decrease follows a curvilinear pattern until a steady value is attained.[66–69] This relaxation can be assigned to bonding breakages under stress over time.[71]

As for the relaxation behavior, illustrated in Figure 12a, the higher is the applied deformation, the higher the reached load level, as expected. Immediately after stretching, the stress induced decreased rapidly at first and then more slowly. As observed during creep testing, a slight decrease in slope during the 1000s holding period was noticed as the PLA content in the structure increased, which is more evident when observing the log–log scale representation of the curves (Figure 12b). Nevertheless, the 16PET braid and the tested hybrid braids still present a low relaxation rate in all strain levels, which means that when elongated, these structures will

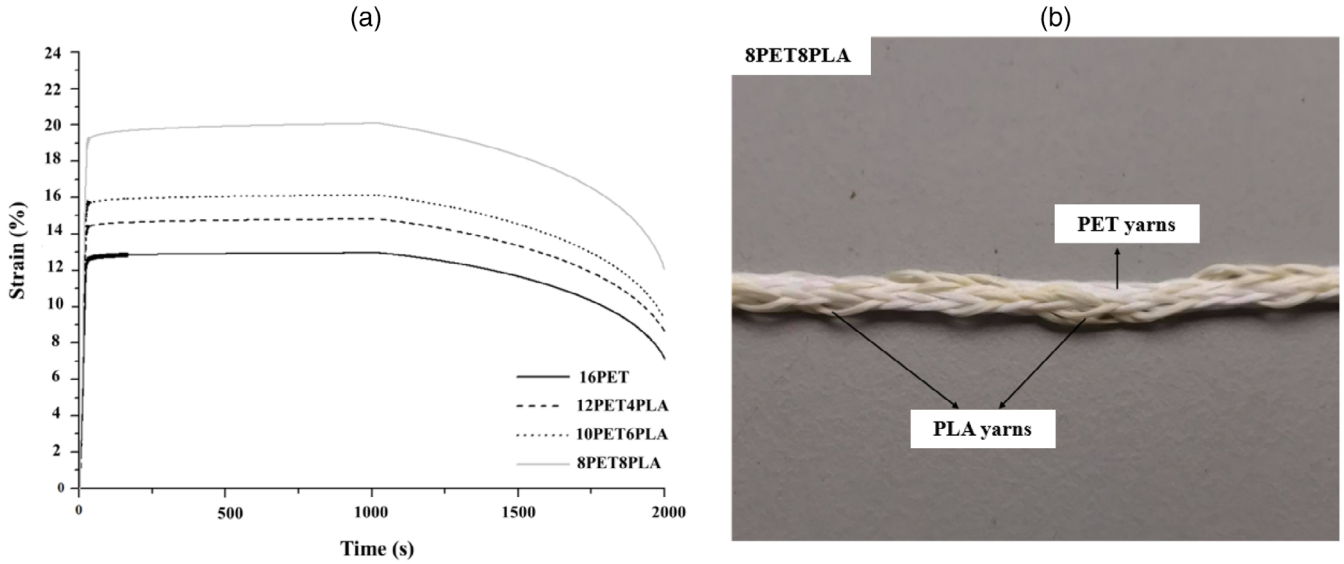

FIGURE 11 (a) Representative curves of creep/recovery behavior of the 16PET and hybrid braided structures at 50% of 16PET braid's breaking force; (b) 8PET8PLA morphology after the creep test [Color figure can be viewed at wileyonlinelibrary.com]

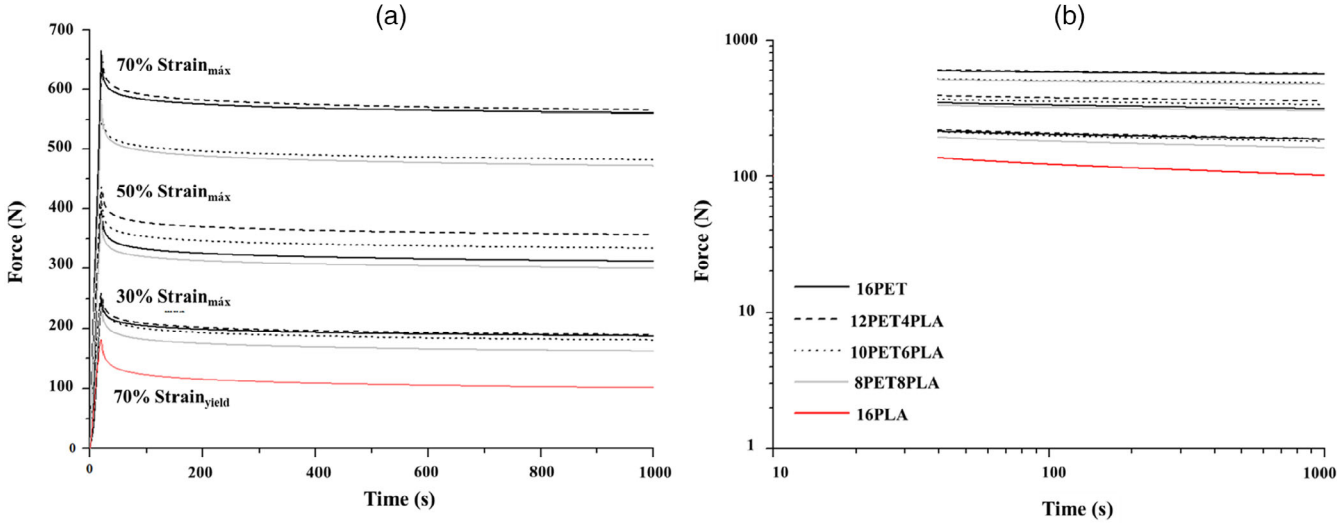

FIGURE 12 (a) Representative curves of relaxation behavior of the braided structures at different levels of force; (b) in log–log scale [Color figure can be viewed at wileyonlinelibrary.com]

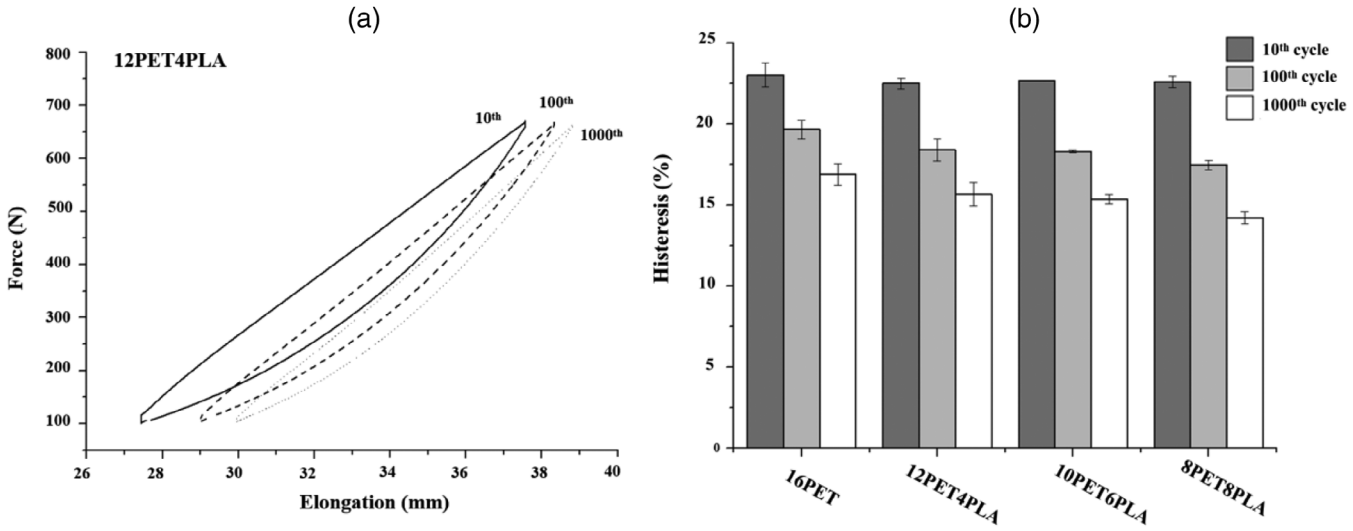

FIGURE 13 (a) Representative hysteresis results of the 12PET4PLA braid force-elongation curves and (b) hysteresis percentage 10, 100, and 1000 cycles

withstand the load over time without getting significantly relaxed. As before, the 16PLA braid demonstrated a higher relaxation rate when subjected to 70% of its yield strain.

Understanding the behavior of the stress relaxation process is essential for the design of a textile scaffold with the required properties for an extended period.[72] The reported data on relaxation behavior at different initial strains may be a good indicator of scaffold recoil after a long-lasting stretch. It was observed that higher PLA content leads to higher relaxation of the textile structure, and this result is relevant for the choice of braid composition for the application envisaged.

The braids under study are intended to sustain long-term repetitive loading, so their mechanical properties after exposure to cyclic loads were evaluated. The structures were subjected to 70% of their breaking force to simulate an extreme loading condition. During a load-deformation cycle, tendons and ligaments display hysteresis,[67] and thus this parameter was evaluated. Hysteresis refers to the loss of energy in a load deformation cycle. The loading-unloading cycles of a tendon are not similar, as the area under the loading curve is greater than the area under the unloading curve, and the difference between both areas represents the energy lost during the load cycle.[67] Hysteresis (%), displayed in Figure 13, was calculated as the area of the loop formed between the load and unload force-elongation curves in the 10th, 100th and 1000th cycles. It appears that after the 10th cycle, the curves' shape stabilizes. This stabilization relates to the structure accommodation since after conditioning, the filaments in the yarns are already stretched in the tensile direction. Similarly, for most tendons/ligaments, a steady state is reached after 10–20 cycles of loading.[67] For each represented cycle, the hysteresis value is low and very similar between the tested samples. Hysteresis values from 5% to 25% have been reported for tendons/ligaments, with most values concentrated at 10%.[66,73] The obtained results are within the reported values. Low hysteresis is favorable for most tendons since they store substantial amounts of elastic energy, which can be used to propel movement.[73]

As the cyclic loading progresses in time, a shift to higher elongation reflects a decrease in stiffness.[67] Indeed, after 1000 cycles of exposure to 70% of each braid breaking force, no significant variations in the measured breaking force and strain at break was detected for all structures, and only a slight decrease in stiffness was observed for the 16PET and hybrid braids (12PET4PLA, 10PET6PLA, 8PET8PLA). However, similar to the creep tests, PLA yarn deformation was widely visible, especially in the 8PET8PLA braid. Even so, as the other braids under study are intended to compose the core of a more complex rope, the presented behavior is a very promising indicator of the rope lifetime.

4 | CONCLUSIONS

In this work, hybrid braided structures produced with PET and PLA multifilament yarns were developed using a textile technique. The obtained porosity and wicking ability were adequate for the intended application. The PET yarns are determinant for the mechanical strength of the hybrid structures, so braids with higher PET content (12PET4PLA and 10PET6PLA braids) presented superior tensile performance, good creep and force-

relaxation behavior, and resistance to cyclic loading, without revealing PLA significant deformation.

The function of different tendons and ligaments varies according to their location. As a result, the requirements in terms of mechanical performance may not be as demanding for specific tissues. The presented hybrid braids are interesting to be used as elementary parts of more complex textile structures that mimic the fibrous structure of different tendons/ligaments. By tailoring the number of braids and the PET:PLA proportion in each braid, the morphology and tensile properties as actual load, strain at failure, and stiffness of a specific tissue can be achieved. The presence of PLA should allow long-term tissue ingrowth and native integration of the structure.

ACKNOWLEDGMENTS

Financial support from PT national funds (FCT/MCTES, Fundação para a Ciência e Tecnologia and Ministério da Ciência, Tecnologia e Ensino Superior) through the project UIDB/50006/2020 is acknowledged by REQUIMTE-LAQV authors. IPC authors acknowledge "National Funds through FCT—Portuguese Foundation for Science and Technology", References UIDB/05256/2020 and UIDP/05256/2020. Tânia Peixoto acknowledges the financial support from FCT and ESF (European Social Fund) through North Portugal Regional Operational Program, through the PhD Grant PD/BD/143035/2018.

DATA AVAILABILITY STATEMENT

No. Research data are not shared.

ORCID

Maria A. Lopes https://orcid.org/0000-0003-4105-8148

REFERENCES

[1] S. P. Lake, Q. Liu, M. Xing, L. E. Iannucci, Z. Wang, C. Zhao, *Principles of Tissue Engineering*, Elsevier, London, UK **2020**, p. 989.
[2] Y. J. No, M. Castilho, Y. Ramaswamy, H. Zreiqat, *Adv. Mater.* **2019**, *32*, 1904511.
[3] S. Chen, J. Wang, Y. Chen, X. Mo, C. Fan, *Mater. Sci. Eng. C* **2021**, *119*, 111506.
[4] A. J. Lomas, C. N. M. Ryan, A. Sorushanova, N. Shologu, A. I. Sideri, V. Tsioli, G. C. Fthenakis, A. Tzora, I. Skoufos, L. R. Quinlan, G. O'Laighin, A. M. Mullen, J. L. Kelly, S. Kearns, M. Biggs, A. Pandit, D. I. Zeugolis, *Adv. Drug Deliv. Rev.* **2015**, *84*, 257.
[5] M. C. Araque-Monrós, D. M. García-Cruz, J. L. Escobar-Ivirico, L. Gil-Santos, M. Monleón-Pradas, J. Más-Estellés, *Ann. Biomed. Eng.* **2020**, *48*, 757.
[6] S. Wu, Y. Wang, P. N. Streubel, B. Duan, *Acta Biomater.* **2017**, *62*, 102.
[7] M. T. Rodrigues, R. L. Reis, M. E. Gomes, *J. Tissue Eng. Regen. Med.* **2013**, *7*, 673.
[8] A. Sensini, C. Gotti, J. Belcari, A. Zucchelli, M. L. Focarete, C. Gualandi, I. Todaro, A. P. Kao, G. Tozzi, L. Cristofolini, *Med. Eng. Phys.* **2019**, *71*, 79.
[9] D. S. Morais, J. Cruz, R. Fangueiro, H. Lopes, R. M. Guedes, M. A. Lopes, *J. Mech. Behav. Biomed. Mater.* **2020**, *106*, 103734.
[10] Y. J. No, S. Tarafder, B. Reischl, Y. Ramaswamy, C. Dunstan, O. Friedrich, C. H. Lee, H. Zreiqat, *ACS Biomater Sci. Eng.* **2020**, *6*, 1887.
[11] W. L. Lim, L. L. Liau, M. H. Ng, S. R. Chowdhury, J. X. Law, *Tissue Eng. Regen. Med.* **2019**, *16*, 549.
[12] R. L. Horan, A. L. Collette, C. Lee, K. Antle, J. Chen, G. H. Altman, *J. Biomech.* **2006**, *39*, 2232.
[13] D. S. Morais, J. Torres, R. M. Guedes, M. A. Lopes, *Ann. Biomed. Eng.* **2015**, *43*, 2025.
[14] I. Manavitehrani, A. Fathi, H. Badr, S. Daly, A. Negahi Shirazi, F. Dehghani, *Polymers* **2016**, *8*, 20.
[15] A. V. Vasiliadis, K. Katakalos, *J. Funct. Biomater.* **2020**, *11*, 78.
[16] D. S. Morais, J. Cruz, R. Fangueiro, M. A. Lopes, R. M. Guedes, *Mech. Mater.* **2021**, *153*, 103668.
[17] T. Tu, Y. Shen, X. Wang, W. Zhang, G. Zhou, Y. Zhang, W. Wang, W. Liu, *Appl. Mater. Today* **2020**, *18*, 100495.
[18] O. Ajala, C. Werther, P. Nikaeen, R. P. Singh, D. Depan, *Polym. Adv. Technol.* **2019**, *30*, 1825.
[19] F. Alshomer, C. Chaves, D. M. Kalaskar, *J. Mater.* **2018**, *2018*, 9868151.
[20] J. S. Bergstroem, D. Hayman, *Ann. Biomed. Eng.* **2016**, *44*, 330.
[21] S. Wu, R. Zhou, F. Zhou, P. N. Streubel, S. Chen, B. Duan, *Mater. Sci. Eng. C* **2020**, *106*, 110268.
[22] Y. Jiao, C. Li, L. Liu, F. Wang, X. Liu, J. Mao, L. Wang, *Biomater. Sci.* **2020**, *8*, 3574.
[23] M. Kun, C. Chan, S. Ramakrishna, A. Kulkarni, K. Vadodaria, *Advanced Textiles for Wound Care*, Elsevier, Duxford, UK **2019**, p. 329.
[24] A. Sensini, L. Cristofolini, *Materials* **2018**, *11*, 1963.
[25] M. Akbari, A. Tamayol, S. Bagherifard, L. Serex, P. Mostafalu, N. Faramarzi, M. H. Mohammadi, A. Khademhosseini, *Adv. Healthc. Mater.* **2016**, *5*, 751.
[26] A. M. Pinto, J. Cabral, D. A. P. Tanaka, A. M. Mendes, F. D. Magalhães, *Polym. Int.* **2013**, *62*, 33.
[27] W. Dong, J. Zhao, C. Li, M. Guo, D. Zhao, Q. Fan, *Polym. Bull.* **2002**, *49*, 197.
[28] T. A. L. Wren, S. A. Yerby, G. S. Beaupré, D. R. Carter, *Clin. Biomech.* **2001**, *16*, 245.
[29] K. Intziegianni, M. Cassel, K. Fröhlich, T. Engel, F. Mayer, *Sport Orthop. Traumatol.* **2015**, *31*, 260.
[30] M. S. Singhvi, S. S. Zinjarde, D. V. Gokhale, *J. Appl. Microbiol.* **2019**, *127*, 1612.
[31] S. L. Edwards, J. A. Werkmeister, *J. Biomed. Mater. Res. Part A* **2012**, *100*, 3326.
[32] Y. Wu, Y. Han, Y. S. Wong, J. Y. H. Fuh, *J. Tissue Eng. Regen. Med.* **2018**, *12*, 1798.
[33] J. R. Sarasua, N. López-Rodríguez, E. Zuza, S. Petisco, B. Castro, M. Del Olmo, P. Teodoro, A. aloznso-varona, *J. Mater. Sci. Mater. Med.* **2011**, *22*, 2513.
[34] M. Yasuniwa, S. Tsubakihara, Y. Sugimoto, C. Nakafuku, *J. Polym. Sci. Part B Polym. Phys.* **2004**, *42*, 25.
[35] F. Ronkay, B. Molnár, D. Nagy, G. Szarka, B. Iván, F. Kristály, V. Mertinger, K. Bocz, *J. Polym. Res.* **2020**, *27*, 1.

[36] C. A. Avila-Orta, F. J. Medellín-Rodríguez, Z.-G. Wang, D. Navarro-Rodríguez, B. S. Hsiao, F. Yeh, *Polymer* **2003**, *44*, 1527.
[37] C. A. Gracia-Fernández, S. Gómez-Barreiro, J. López-Beceiro, S. Naya, R. Artiaga, *J. Mater. Res.* **2012**, *27*, 1379.
[38] K. De Clerck, H. Rahier, B. Van Mele, P. Kiekens, *J. Appl. Polym. Sci.* **2003**, *89*, 3840.
[39] C. M. Clarkson, S. M. El Awad Azrak, R. Chowdhury, S. N. Shuvo, J. Snyder, G. Schueneman, V. Ortalan, J. P. Youngblood, *ACS Appl. Polym. Mater.* **2019**, *1*, 160.
[40] N. Özdil, G. Ö. Kayseri, G. S. Mengüç, *Abrasion Resist. Mater.* **2012**, 119.
[41] F. Ning, G. He, C. Sheng, H. He, J. Wang, R. Zhou, X. Ning, *J. Eng. Fiber Fabr.* **2021**, *16*, 1.
[42] S. Das, *J. Nat. Fibers* **2020**, 1.
[43] Ö. Özdemir, E. K. Çeven, *Text. Res. J.* **2004**, *74*, 515.
[44] S. Altaş, B. Ozgen, *J. Text. Inst.* **2016**, *107*, 1232.
[45] J. S. Dugan, *Int. Nonwovens J.* **2001**, *3*, 29.
[46] S. Ghosh, S. Krishnan, *Indian J. Fibre Text. Res.* **2007**, *32*, 119.
[47] G. Krupincová, J. Hatipoglu, *Autex Res J.* **2013**, *13*, 22.
[48] S. Khalaj Amnieh, P. Mosaddegh, M. Mashayekhi, M. Kharaziha, *J. Appl. Polym. Sci.* **2021**, *138*, 50389.
[49] G. Gorrasi, R. Pantani, *Synthesis, Structure and Properties of Poly(Lactic Acid)*, Vol. 279, Springer, Cham, Switzerland **2017**, p. 119.
[50] F. Dubelley, E. Planes, C. Bas, E. Pons, B. Yrieix, L. Flandin, *Polymer* **2018**, *142*, 285.
[51] E. Pirzadeh, A. Zadhoush, M. Haghighat, *J. Appl. Polym. Sci.* **2007**, *106*, 1544.
[52] M. Arhant, M. Le Gall, P.-Y. Le Gac, P. Davies, *Polym. Degrad. Stab.* **2019**, *161*, 175.
[53] S. Rana, R. Fangueiro, *Braided Structures and Composites: Production, Properties, Mechanics, and Technical Applications*, CRC Press, Boca Raton, FL **2015**.
[54] A. Rawal, H. Saraswat, A. Sibal, *Text. Res. J.* **2015**, *85*, 2083.
[55] A. Rawal, P. Potluri, C. Steele, *J. Ind. Text.* **2005**, *35*, 115.
[56] R. Fangueiro, F. Soutinho, *Fibrous and Composite Materials for Civil Engineering Applications*, Woodhead Publishing, Cambridge, UK **2011**, p. 62.
[57] J. Hajrasouliha, R. J. Nedoushan, M. Sheikhzadeh, W. Na, W.-R. Yu, *J. Compos. Mater.* **2018**, *52*, 4009.
[58] N. Sultana, T. H. Khan, *J. Nanomater.* **2013**, *2013*, 479109.
[59] B. Kumar, A. Das, *Fibers Polym.* **2014**, *15*, 625.
[60] G. Hochleitner, F. Chen, C. Blum, P. D. Dalton, B. Amsden, J. Groll, *Acta Biomater.* **2018**, *72*, 110.
[61] T. Sang, C. J. Wallis, G. Hill, G. J. P. Britovsek, *Eur. Polym. J.* **2020**, *136*, 109873.
[62] Y. Chen, X. Ding, Y. Li, *Fibers Polym.* **2012**, *13*, 169.
[63] R. M. Felfel, K. M. Z. Hossain, A. J. Parsons, C. D. Rudd, I. Ahmed, *J. Mater. Sci.* **2015**, *50*, 3942.
[64] M. C. Araque-Monrós, A. Vidaurre, L. Gil-Santos, S. G. Bernabé, M. Monleón-Pradas, J. Más-Estellés, *Polym. Degrad. Stab.* **2013**, *98*, 1563.
[65] V. G. L. Souza, A. L. Fernando, *Food Packag. Shelf Life* **2016**, *8*, 63.
[66] C. N. Maganaris, M. V. Narici, *Tendon Injuries*, Springer, London, UK **2005**, p. 14.
[67] R. B. Martin, D. B. Burr, N. A. Sharkey, D. P. Fyhrie, *Skeletal Tissue Mechanics*, Springer, New York **2015**, p. 175.
[68] Cerrada ML. Introduction to the Viscoelastic Response in Polymers. In Proc. of the Thermal Analysis, Fundamentals and Applications to Material Characterization; **2005**; 167–182.
[69] K. Balani, V. Verma, A. Agarwal, R. Narayan, *Biosurfaces: A Materials Science and Engineering Perspective*, John Wiley & Sons, Inc., Hoboken, NJ **2015**, pp. 329-344.
[70] D. Hawkins, C. Lum, D. Gaydos, R. Dunning, *J. Biomech.* **2009**, *42*, 2813.
[71] A. M. Manich, R. Miguel, J. Lucas, F. Franco, B. Baena, J. Carilla, L. Montero, D. Cayuela, *Text. Res. J.* **2011**, *81*, 1788.
[72] G. Laureckienė, R. Milašius, *Autex Res. J.* **2017**, *17*, 379.
[73] J. Peltonen, N. J. Cronin, L. Stenroth, T. Finni, J. Avela, *Springerplus* **2013**, *2*, 1.

How to cite this article: T. Peixoto, S. Carneiro, R. Fangueiro, R. M. Guedes, M. C. Paiva, M. A. Lopes, *J. Appl. Polym. Sci.* **2021**, e52013. https://doi.org/10.1002/app.52013